Agricultural and Forest Meteorology 184 (2014) 220–229

Contents lists available at ScienceDirect

Agricultural and Forest Meteorology

journal homepage: www.elsevier.com/locate/agrformet

# A robust videogrametric method for the velocimetry of wind-induced motion in trees

Adelin Barbacci[a], Julien Diener[c], Pascal Hémon[c], Boris Adam[a], Nicolas Donès[a], Lionel Reveret[d], Bruno Moulia[a,b,*]

[a] INRA (Institut National de la Recherche Agronomique), UMR0547 PIAF (Unité Mixte de Recherche Physique et Physiologie Intégratives de l'Arbre Fruitier et Forestier), F-63100 Clermont-Ferrand, France
[b] Clermont Université, Université Blaise Pascal, UMR0547 PIAF (Unité Mixte de Recherche Physique et Physiologie Intégratives de l'Arbre Fruitier et Forestier), BP 10448, F-63000 Clermont-Ferrand, France
[c] Department of Mechanics, LadHyX, Ecole Polytechnique-CNRS, F-91128 Palaiseau, France
[d] UMR 5224 LJK, INRIA Rhône-Alpes, Universités Grenoble PIAF, INRA, 5 Chemin de Beaulieu, 63039 Clermont-Ferrand, France

ARTICLE INFO

*Article history:*
Received 15 April 2013
Received in revised form
12 September 2013
Accepted 8 October 2013

*Keywords:*
Wind
PIV
Tracking method
Biomechanics
Motion

ABSTRACT

Wind has major effect on plants, from growth changes to windbreaks. Therefore, there is a crucial need for non-invasive methods to describe and quantify the complex motion of a plant induced by wind. In this paper two methods based on video sequences analysis are studied. An adaptation of the classical Particle Image Velocimetry method (nat-PIV) is compared with a tracking method based on the optical flow method of Lukas and Kanade, initialized with the features selection method of Shi and Tomasi (ST + KLT). Both methods were benchmarked on an experiment on a walnut tree in open-field conditions submitted to different wind flows at different periods of the year and equipped with 3D magnetic tracking. The metrological assessment was performed in two steps. We first tested if the results given by both methods were significantly different. Secondly, a direct assessment of the two methods versus 3D magnetic tracking was performed. The ST + KLT method proved to be more accurate and robust than nat-PIV one. The outputs of the ST + KLT method are independent of the foliage density, wind velocity and of light gradient intrinsic to outdoor scene. The implementation of ST + KLT method developed for this study in Matlab is freely available.



## 1. Introduction

Wind hazards on plants are a major problem in agriculture and forestry because of the yield losses they entail (Berry et al., 2003; de Langre, 2008; Gardiner, 2000). For example annual yield losses due to lodging in cereals amounts 20% world wide despite the selection of short-sized genotypes. In forestry, recurrent storms damages have emphasized the need for forest management limiting damage to trees (Achim et al., 2005). This has fostered a long-term interest on the biomechanics of wind–plant interaction (see rev in Moulia and Fournier, 1997; Gardiner et al., 2008; de Langre, 2006). For windbreaks, it has been shown that the dynamic component of wind loading and the inertial loads due to wind induced accelerations must be considered (Gardiner, 2000). Moreover, branches may reach their breaking limits before the basis of the trunk, acting as security fuses (Hedden et al., 1995; Niklas and Spatz, 2000; Lopez et al., 2011). Wind is also influencing plant growth, through gas exchanges (de Langre, 2006).

Finally the deformations induced by chronic winds are sensed by the plant, giving rise to an acclimation and hardening growth process called thigmomorphogenesis (reviewed in Moulia et al., 2011). This includes dramatic change in growth in height and girth, as well as the production of special woods such as flexure wood and eventually, when non-elastic bending/tilting, occurs, reaction wood (Telewski, 2006).

The motion and deformation of plants under the wind can be complex, and depends both on the architecture of the plant (Sellier et al., 2006; Rodriguez et al., 2008) and on its environment (e.g. isolated tree vs trees in a forest canopy, de Langre, 2008) For example the wind–canopy interaction is initiated by the Kelvin–Helmoltz instability (Raupach et al., 1996) shedding a cascade of vortex waves called Honamis (Py et al., 2005; Dupont et al., 2010). Additionally the response of the plant itself may be complex. Indeed many

*Abbreviations:* nat-PIV, Particle Image Velocimetry method over natural texture; ST + KLT, Lukas Kanade method coupled with Shi and Thomasi features selection; *ts*, abbreviation used to describe a condition of the test set $ts \in \{DHighW, DMediumW, IHighW, IInterW\}$; Meth, suffix corresponding to the method used to compute the velocimetry field. $Meth \in \{OPt, Magnetic\}$ and $Opt \in \{ST+KLT, nat\text{-}PIV\}$.

* Corresponding author. Present address: PIAF, INRA, 5 Chemin de Beaulieu, 63039 Clermont-Ferrand, France. Tel.: +33 473 62 44 74; fax: +33 473 62 44 54.
*E-mail address:* bruno.moulia@clermont.inra.fr (B. Moulia).

0168-1923/$ – see front matter © 2013 Elsevier B.V. All rights reserved.
http://dx.doi.org/10.1016/j.agrformet.2013.10.003

**Nomenclature**

*Velocimetry notations*

| | |
|---|---|
| $V_{ts,Meth} = V_{ts,Meth}(x,y,t)$ | velocimetry vector field obtains for all the sequences corresponding to the test set ts with the method *Meth*. The coordinates *x*,*y* corresponding to the geometrical center of grid unit; *t* is the time |
| $\langle V_{ts,Meth} \rangle$ | spatial and temporal average of the velocimetry obtained by the method *Meth* for the test set *ts* |
| $\overline{V_{ts,Meth}}$ | temporal mean of the velocimetry calculated to compare nat-PIV and ST + KLT measurements with magnetic ones |
| $\tau_c$, $\tau_{rs}$ | time periods of the camera (0.04 s) and commun time period to magnetic and numeric measurements (0.2 s) |

*Statistical treatments*

| | |
|---|---|
| $a_{ts}$ | slope of the orthogonal regression lines |
| $a_{ts,sup}$ $a_{ts,inf}$ | the confidence interval of the slope |
| $b_{ts}$ | intercept of the orthogonal regression lines |
| $R_{ts}$ | correlation coefficient |

modes of wind-induced vibrations can be characterized (Sellier et al., 2006; Rodriguez et al., 2008).

Different models for the various wind-induced effects have been developed (e.g. Sellier and Fourcaud, 2005; Py et al., 2006; Gardiner et al., 2008; Rodriguez et al., 2008; Dupont and Brunet, 2007; Moulia et al., 2011), some of them including the motion and deformation of all the branches (e.g. Sellier and Fourcaud, 2005; Rodriguez et al., 2008) or of a continuous canopy (Py et al., 2006; Dupont et al., 2010). However to date measurements of wind-induced motions were not obtained with such a detail. In most case, only local displacement were measured by mean of inclinometers, strain gauges and laser-beam (Flesch and Grant, 1992a, 1992b; Hassinen et al., 1998; Sterling et al., 2003; Sellier et al., 2006) or, more recently, through a set of magnetic 3D trackers (Rudnicki and Burns, 2006; de Langre et al., 2012). Local measurements do not allow for a characterization of many features of wind induced motion in plants. Honamis or vibration modes can hardly be characterized (Py et al., 2005) nor the signal triggering the plant thigmomorphogenesis, that involves a spatial integration of the strain field over the whole plant (Moulia et al., 2011). Moreover some plant organs (e.g. small branches, leaves) may be light-weighted and the mass or the geometry of some sensors may alter the dynamics of the plant.

There is thus a crucial need for a more extensive description of wind induced motion by a non-invasive velocimetric characterization, i.e. the quantification of the spatio-temporal vector field of the velocity of motion of the different plant parts. Velocimetric non-invasive measurements using video images videogrametric analyses are standard in fluid and solid mechanics with the widespread use of Particle Image Velocimetry (PIV, Raffel et al., 2002). Concurrently, another type of methods based on optic flow has been developed independently in the area of computer vision (Baker and Matthews, 2004). Although related, the principles and software implementation of these methods differ. The image-processing algorithm of the PIV belongs to the block-matching methods since it is based on the computation of the cross-correlation between image patches in sequential images. In it standard use in fluid mechanics, it usually requires the seeding of the moving flow with artificial markers and specialized and controlled laser lighting, so that the texture of the images meets the assumptions of the PIV algorithm. Optical flow methods are based on the assumption that changes in the gray-level intensities of sets of pixels between successive images results from the (unknown) motion of the material particles in the scene relative to the camera.

PIV has been mostly used for the measurement of fluid flows. Optic flow methods (Horn and Schunck, 1981) have being applied to many complex scenes including moving people, crafts or animals. In particular a robust algorithm proposed by Lukas and Kanade (LK) (Lucas and Kanade, 1981) has been used widely and has been improved by the definition of a pretreatment to LK detecting the "good features to track" in the sequence for a more accurate velocimetry (Shi and Tomasi, 1994, this methods will be noted ST + KLT in the following). In ST + KLT the "good features to track" are defined as displaying orthogonal gray-level gradients, so that their tracking can be optimal in every direction.

These methods are known to have different advantages and drawbacks. The PIV method outputs dense velocity fields. But it may be sensitive to the texture of the image and displays possible peak locking, a systematic tendency to bias toward integer values of motion when the pixelisation of the image is too coarse relative to the amplitude of the motion. Multipass algorithms are used to improve resolution and to decrease peak-locking but require extensive computation time. The KLT method is computationally much faster thanks to the linearization of the equation determining the velocity between two consecutive frames. However, this linearization may introduce critical instability at locations where the images shows poor texture. Moreover it is prone to the aperture problem which is an optical illusion making the local determination of the movement impossible. These two limitations can be solved using a features selection such as in Shi and Tomasi (1994). However, this features – selection step makes the ST + KLT outputs sparse. Finally both methods, PIV and ST + KLT, assume small displacements between successive images, although a standard multi-resolution implementation of KLT allows larger displacement to be handled (Bouguet, 2000; Bradski, 2000).

A modified PIV method using foliage as natural texturing markers (noted nat-PIV thereafter) has been instrumental in characterizing honami-induced velocity field of plant tips in dense canopies of alfalfa and wheat crops (Py et al., 2005). And this unique data set has been used to assess several wind–canopy interaction models (Py et al., 2005; Dupont and Brunet, 2007; Dupont et al., 2010). However, the study of homogeneous dense crops is likely to be the simplest case to be studied, as the top of a dense plant canopy is often planar and displays mostly 2D motion. In most cases though, the structure of the scene of interest may be much more complex. Canopy can be sparse, and isolated plants with complex structure such as trees need to be considered (Sellier et al., 2006; Rudnicki et al., 2001). Additionally, the amount and colors of foliage elements can vary widely over the seasons.

A proof-of-concept test for the use of the ST + KLT method to analyze has been conducted on a few complex isolated plants such as bonsai tree (Diener et al., 2006).

However none of these two methods have been submitted to metrological assessment for the wind-induced motion of complex plants structures in different conditions of wind, foliage and background. Moreover the criteria of choice for one method vs another are unclear. Is there one robust and versatile method for velocimetric measurements of plant motion, or are the two types of methods complementary? Is there a method that is more accurate? Does this depend on wind intensity or on the amount of foliage? Do variations in the amount of lighting over space and time or the background (sky, soil) alter the measurement?

The aim of the paper was thus to assess and compare the two methods versus reference magnetic tracking measurement in a combination of wind, foliage, lighting and background. This "benchmarking" was conducted in the most challenging configuration; namely a complex tree in the field, with natural lighting and changing sky background, in a sample of different weathers and seasonal

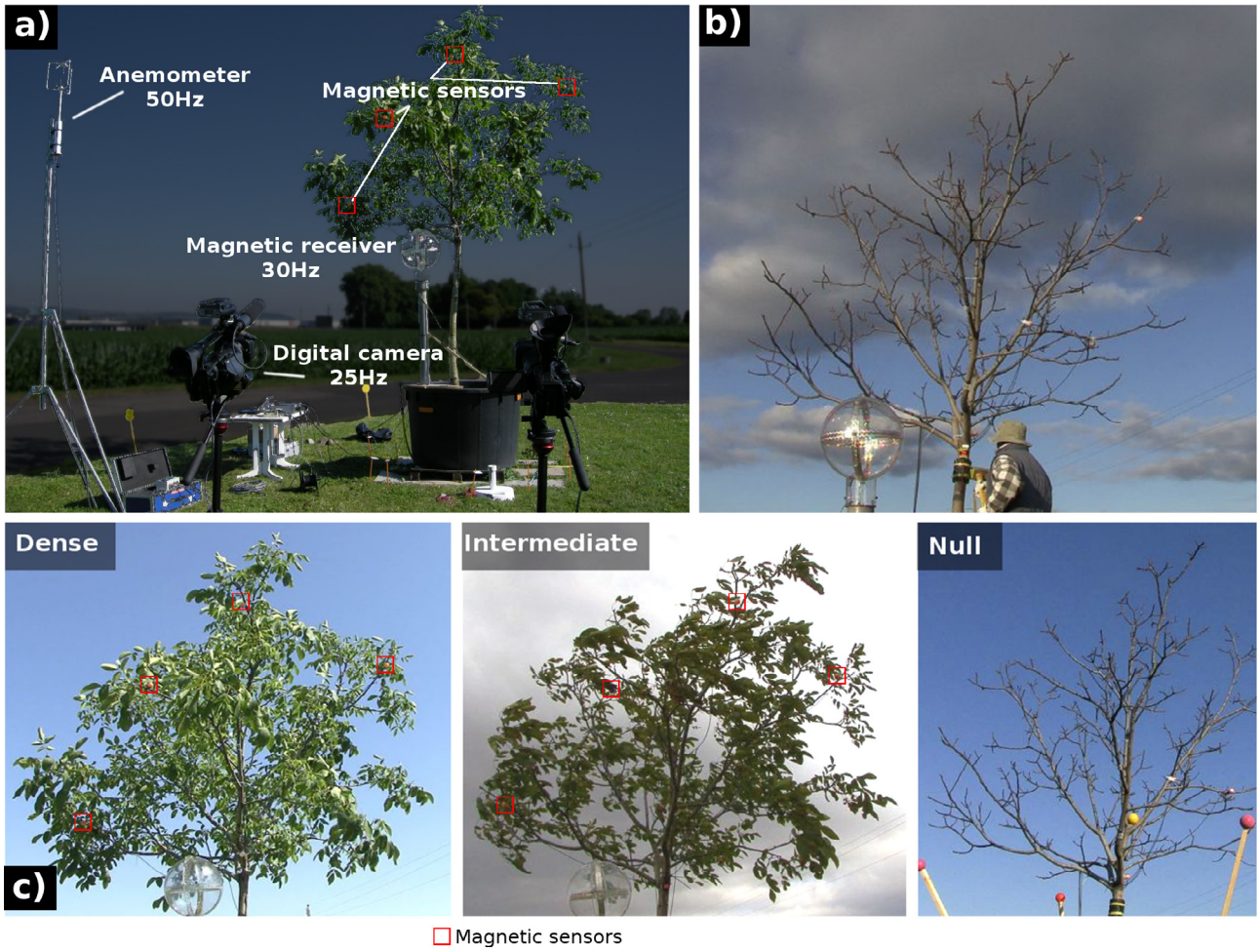


**Fig. 1.** (a) Raw-data acquisition. A computer triggered an anemometer (measurement frequency 50 Hz), (a) Polhemus fastrack (measurement frequency 30 Hz). The computer lights a red diode panel in order to determine the beginning of the image sequence for the digital camera (measurement frequency 25 Hz). (b) Null + Inert conditions (see also supplementary data 2). The motion is created manually by exciting the tree vibrations through impacts and pull and release (c) 3 pictures of the set-up, note that the sky in the background and the lighting can be very variable, as well as the amount of foliage.

foliage situations all through the year. Our hypothesis was that reliable estimates of the velocity fields will be obtained using optical velocimetric methods, but that the best methods will be condition-dependent: i.e. nat-PIV would be more efficient for dense foliages, and that the ST + KLT method would only be efficient with obvious angular features such as in the leafless tree.

Here we however show that the ST + KLT method provides a robust and accurate measurement in all the conditions. Moreover a user-friendly versatile software Kineplant-CRToolbox is now available for use by plant biomechanicians, micrometerologists or biologists (http://sites.google.com/site/crtoolbox).

## 2. Materials and methods

### 2.1. Plant material and scene

A 10-year-old walnut tree (*Juglans regia* L.) (Height = 4.2 m Dbh = 7.7 cm) was used for this experiment (Fig. 1). It was grown in pot (height of the tree collar = 80 cm above ground) and then located outdoor, in openfield conditions at Clermont-Ferrand France (N 45.77482° E 3.14414°). The 3D architecture and the vibration modes of this walnut tree have been fully characterized on the same year as the present experiment (early fall 2008) by Rodriguez et al. (2012).

### 2.2. Measurements and raw data acquisition

To use nat-PIV and ST + KLT methods we need: (i) images sequences of the wind-induced motion of the tree, (ii) a reference measurement allowing the comparison with the velocity fields given by the two videogrametric methods and (iii) wind velocity, in order to assess the dependency of nat-PIV and ST + KLT methods on wind intensity.

The global setting of the experiment is given in Fig. 1a.

Video acquisition was achieved using a video-camera (Sony HVR-V1, format HDV 1080i) located at approximately 4 m from the base of the tree and at 1.5 m height. The frequency of frame acquisition was 25 fps progressive scan (or Hz) and the spatial resolution was 1440 × 1080 pixels. The focal length was set at 3.9 mm at constant diaphragm (e.g. supplementary data 1). Care was taken to secure the tripods of the cameras to minimize the amplitude of possible wind-induced motion and to ensure resonant frequencies high enough to not interfere with the measurements. Two cameras were placed in parallel in order to enhance the reliability of the shooting. This stereoscopic acquisition may be used in the future to reconstruct and analyze 3D motion. But as a requisite for a proper 3D analysis is to have reliable 2D analyses in the two cameras, the benchmarking for motion measurements was performed only in 2D.

The reference method was provided using a 3D magnetic tracker (Polhemus 3space Fastrack, Polhemus Inc, Colchester, VT, USA), as described in de Langre et al. (2012). Briefly, this measurement involves the generation of 3 alternative and orthogonal magnetic fields by 3 toric magnetic sources set on a Plexiglas sphere (Polhemus Long range, see Fig. 1a) and the recording of the induced current in 3 orthogonal coils in the receivers or sensors. As the induced current depends on distance to the source and on the orientation of the coils, the equations for the 3D position (and Euler orientation angles) of the receivers can be solved. Four magnetic sensors (Polhemus fastrack) were disposed in the crown of the tree so that there were visible from the cameras. The position of the 4 sensors was chosen to sample the whole span of the crown in order to allow a robust camera calibration (see Section 2.4). In order to enhance the visibility of the receivers on the video, they were inserted in fluo-red ping-pong balls. The mass of each receiver is 20 g. The source sphere was positioned on top of the pot, approximately at the mid height of the tree trunk (and at 0.5 m horizontal distance from it). Data acquisition was performed at 30 Hz.

Wind speed and direction data were obtained using a 3-axis ultrasonic anemometers R3 (R3-50 Professional 3D Anemometer, Gill Instrument) with the frequency set at 50 Hz. It was positioned at the height of the center of the tree crown (3.5 m height from ground) on the wind-ward side of the tree, at a tradeoff distance (6 m) so to avoid wake effects on the tree but to give relevant information of the mean wind conditions over the tree during the run of a video sequence. The wind velocity vector pointing into the direction of the tree was then computed from the wind data.

These 3 measurements (i.e. video recording, magnetic tracking and wind speed) were conjointly performed. Magnetic tracking and wind speed acquisition were triggered by a laptop and directly stored on its hard drive using the PIAFDigitTrack software developed for this work by Donès and Adam (2008). The synchronization with the video was achieved by the switching on (resp. off) of a red led panel set on top of the tree trunk when the start (resp. stop) signal was sent by the computer to the magnetic tracker and the anemometer. The spatial position of the camera, the anemometer and the cameras were recorded using an electronic theodolite (ER R100M Leica).

The part of the movie, during while the red led panel was on, was decomposed into image sequence with the freeware MEncoder (http://www.mplayerhq.hu/design7/news.html). Each frame was spatially interpolated by Lanczos algorithm to obtain a $1980 \times 1080$ image with isometric aspect. Pictures were stored in bmp format.

### 2.3. Experimental design and test sets

To test the influence of the texture of the image and of the magnitude of displacements on the velocimetry fields output by the two videogrametric methods, images sequences were shot for different foliage and wind situations (Table 1). The experiments were conducted over three weeks at three seasons along the year 2008: early summer (July 07–11), early fall (September 29–October 03), winter (December 08–12).

Three classes of foliage texture were thereby produced (Fig. 1c) noted Dense (D-), Intermediate (I-) and Null. Dense foliage was obtained in summer, when the tree has many green leaves; the Intermediate foliage was obtained in the fall when the number of leaves was smaller and their colors turned to orange, and the Null foliage in winter after the fall of all foliage. However, in winter that year, the drag force by wind was insufficient to bring significant motion. Movements of small intensity were then created manually by exciting tree vibrations through repeated pull and release loadings (Rodriguez et al., 2012) and impacts (inducing the whole spectrum of vibration modes). In the Dense and Intermediate foliate situations, the wind data were clustered using a k-mean algorithm and two clusters of contrasted mean wind speed conditions were retained, and noted HighW and MediumW (and the corresponding video sequences sorted in the image database). The mean wind velocities in each of the wind-speed condition were the same for the two seasons (Table 1) and the difference between the mean wind velocity in HighW and MediumW was approx. 30%. Note however that the actual fluctuant drag on the tree can also vary with the amount and density of foliage, so that similar wind speeds at different season do not mean similar drag forces. Finally the combination of foliage density and wind speed conditions resulted in four test sets, listed in Table 1. In all the cases the dominant wind was mostly coming from the West-South-West, i.e. parallel to the image plane. The winter set with no foliage and inertial motion is an extra test set, corresponding to an extreme case of texture and magnitude. This test-set, noted NullW + Inert (for inertial motion) is meant to be the most challenging and extreme test for the velocimetric methods, because of the small and transient displacements and the lack of foliage elements. But it was treated separately, as it does not assess natural situations.

### 2.4. Comparison with ground truth data

The positions of the sensors measured by 3D magnetic tracking were then projected on the 2D reference frame of the image to allow the quantitative comparison between the video velocimetric methods and the magnetic tracking of the sensors.

The images we calibrated in the objective reference frame of the 3D magnetic tracker and scaled from pixel/s to $m/\tau_{rs}$ (ground truth data) with $\tau_{rs}$ a time period (to be defined below). This was done using the position of the 4 sensors at different times, which can be computed both in the reference frame of the tracker and in every image.

The time resolution of the magnetic measurement (0.0333 s) and of the image sequence (0.04 s) was different. Each 0.2 s both methods shared a measurement. So a new velocimetry was computed for each shared instant by averaging velocimetry on the common time period $\tau_{rs}$.

Hence $\bar{V}_{ts,Magn} = \frac{1}{6}\sum_{t=t_0}^{t=t_0+5} V_{ts,Magn}$ and $\bar{V}_{ts,Num} = \frac{1}{5}\sum_{t=t_0}^{t=t_0+4} V_{ts,Num}$ are the new velocimetry fields used to compare optical and magnetical velocimetry fields.

The camera matrix is a $3 \times 4$ matrix defined as

$$\begin{pmatrix} x \\ y \\ 1 \end{pmatrix} = \begin{pmatrix} m_{11} & m_{12} & m_{13} & m_{14} \\ m_{21} & m_{22} & m_{23} & m_{24} \\ m_{31} & m_{32} & m_{33} & m_{34} \end{pmatrix} \begin{pmatrix} X \\ Y \\ Z \\ 1 \end{pmatrix}$$

where $(x,y,1)^T$ are the homogeneous coordinates of a sensor in the reference frame of the image (in pixel) and $(X,Y,Z,1)^T$ the homogeneous coordinates of the same sensor in the magnetic reference frame (in meter). The camera matrix parameters describe the intrinsic parameters of the camera (its focal length, its image sensor size, its principal point) and the extrinsic parameters defining the position of the camera center and the camera's heading in world coordinate. A camera matrix was computed for each digital sequence by a least squares fit, using the positions of the 4 sensors at 6 different times (to minimize the standard error).

### 2.5. Optical velocimetry methods

#### 2.5.1. nat-PIV

In fluid mechanics, PIV usually refers to a complete experimental setting including the lighting, the camera, the seeding and the image correlation algorithm. In the following, nat-PIV only refers to the image correlation algorithm allowing the computation of

**Table 1**
Summary of the test sets analyzed by conditions of wind and foliage density.

| Wind intensity | High (mean 4.72 m/s max 7.79 m/s) | Medium (mean 3.45 m/s max 5.5 m/s) |
|---|---|---|
| Foliage density | | |
| Dense | Noted: DHighW<br>Number of sequence: 2<br>Mean time of a sequence: 24.48 s | Noted: DMediumW<br>Number of sequence: 2<br>Mean time of a sequence: 25.12 s |
| Intermediate | Noted: IHighW<br>Number of sequence: 2<br>Mean time of a sequence: 27.64 s | Noted: IMediumW<br>Number of sequence: 2<br>Mean time of a sequence: 19.02 s |

velocimetry fields from images sequences recorded in natural conditions (Fig. 1).

The nat-PIV algorithm processes pairs of successive gray-scaled frames (Fig. 2). The images are divided into small subwindows called interrogation windows. A spatial correlation is then computed on each pair of interrogation windows. The distance covered by a point between two successive frames is given by the maximum of this correlation function. The velocimetry is then computed by dividing this distance by the time between two frames (in our case $\tau_c = 0.04$ s). This treatment is repeated for each subwindows. A partial overlap of the subwindows allows increasing the spatial resolution of the flow grid.

Improvements to this basic PIV method have been proposed (Carr et al., 2009; Cholemari, 2007; Christensen, 2004). Most of them however require an a priori knowledge on the motion to correct the PIV results. In our case, the wind flow and leaf motion are unknown and such correction could not be used. Thus, a standard implementation in Matlab of PIV algorithm called MatPIV proposed by Sveen (2004) was retained (freely available on http://folk.uio.no/jks/matpiv/index2.html) and included in the Kineplant CR Toolbox.

The MatPIV algorithm, was run in single precision, the size of interrogation windows was $16 \times 16$ pixels and the overlap from interrogation window to interrogation window was 50% (Py et al., 2005). At the end of the run, the outliers were removed using MathPIV *localfilt* and *globlfilt* methods. The computation time was approximately 60 s for two successive frames.

### 2.5.2. ST + KLT

LK method is an optical flow method, a classical method in computer vision (Bouguet, 2000). In this method the cause of the local changes in gray level intensity is assumed to be relative motion between the camera and the tree. The material derivative of the change in gray level is thus zero and at some point in the image the local derivative of the gray level intensity is equal to the motion velocity times the spatial gradient of gray level intensity, allowing the motion to be estimated, i.e.

$$\frac{DI(X,t)}{Dt} = \frac{\partial I}{\partial t} + V \cdot \nabla X = 0 \Rightarrow V = -\frac{\partial I}{\partial t \nabla X}$$

where $D$ is the symbol for the material derivative, $\partial$ is the symbol for the partial local derivative, $I$ is the local gray level intensity, $V$ is the velocity field for the relative motion (optical flow) and $X$ is the spatial coordinates in the image (eulerian specification). Similarly to nat-PIV, the computation of velocimetry is done on two successive greyscaled images (Fig. 2). The ST + KLT module in the Kineplant CR Toolbox is based on an algorithm proposed by Bouguet (2000). Additionally, a preprocessing step was introduced that detects features having high intensity gradients so as to eliminate instability in the tracking. This was based on what Shi and Tomasi, coined as "good features to track" (Shi and Tomasi, 1994) through the method implemented by Bouguet (2000). A pixel is considered to be a good feature if it belongs to a corner, i.e. a two directional change in grayscale intensity.

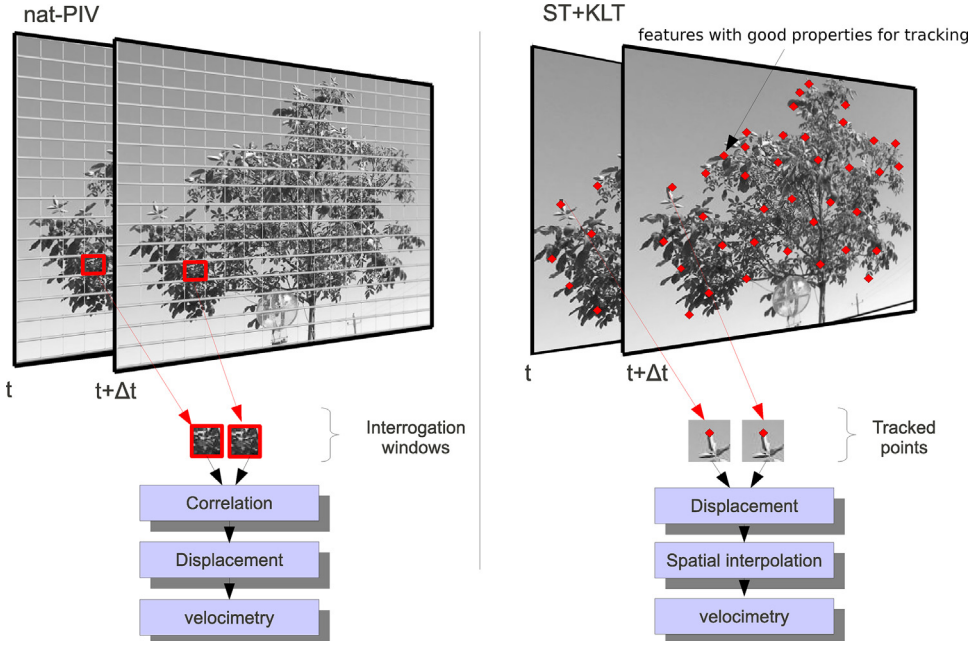


**Fig. 2.** Rational of nat-PIV and ST + KLT algorithms. nat-PIV is based on the cross correlation of subwindows whereas ST + KLT is based on the direct difference between two features with good properties for tracking (high intensity gradients). The density of the output given by ST + KLT method is modified using a spatial interpolation step.

This step solves partially the aperture problem, a classical problem of motion perception in which the motion of a granting pattern is observed through a local observation window (aperture). In this case only the motion component transverse to the granting can be resolved, making the determination of the complete motion impossible since many global movements could generate the same local movement observed through the aperture (e.g. Stoner and Albright, 1996).

A parameter setting the minimal distance between two good features has been introduced to limit the number of tracked point. We set this distance to 6 pixels. Another parameter is the size of the average window to solve for the linearized equation of optical flow, which describes the change of pixel value due to the relative motion between the camera and the tree. We set this window to a square of 16 pixels wide. A hierarchical search (2 levels in our case), for different sub-pixel resolution decreases the computation time and improves robustness. Due to the features selection step, ST + KLT provides a less dense velocimetry field than nat-PIV. In order to compare ST + KLT with nat-PIV, each picture was divided in subwindows of the same size as that of the nat-PIV interrogation windows and a velocimetry vector for the subwindow was computed as a weighted-average of all the ST + KLT tracked features belonging to these subwindows.

The time of computation for 2 consecutive frames with ST + KLT was less than 8 s, i.e. approximately 10 times smaller than the one for nat-PIV.

#### 2.5.3. The Kineplant-CR Toolbox

To allow for a homogeneous and straightforward processing of the images for the two methods, both the nat-PIV and the ST + KLT algorithms were integrated in an user-friendly versatile software Kineplant-CRToolbox (Diener et al., 2012). This software was developed by J Diener and L Reveret and implements Graphic User Interfaces, image pile management and the nat-PIV and the ST + KLT algorithms and is freely available on http://sites.google.com/site/crtoolbox (with tutorial and documentation).

### 2.6. Comparisons of the performances of the velocimetric methods

#### 2.6.1. Comparison with the Magnetic velocimetric method

Magnetic velocimetry only gives an estimate of the motion at the sensors (see Fig. 1). The comparison between Magnetic velocimetry and the two optical velocimetric methods was thus performed locally in the vicinity of these sensors.

In our experiment, 2 sensors were set at approximately 1 m from the receiver whilst the others were set at more than 2 m. The spatial resolution of the sensor displacement is approximately a third order polynomial function of the distance between the sensor and the magnetic receiver (Fig. 3 from Polhemus documentation). Thus the error on the individual position (standard deviation) for the closest sensors was lower than 2.5 mm but it was greater than 1 cm for the others. So only the 2 closest sensors were used for the assessment of the two velocimetric methods (the two others were only used for image calibration see Section 2.4).

An ImageJ plugin (http://rsbweb.nih.gov/ij/) was created to find the sensor position on frames. As the sensors were set inside small fluo-red balls, the segmentation plugin uses the red component to extract the position of sensors. A pixel is tagged as belonging to a sensor when the red value of a pixel was superior to a threshold value. To detect each of the sensors, the tagged pixels were clustered. To do so, the distance between the current pixel and the previously detected pixels was computed. The pixel was then grouped with the closest group of pixel (supplementary data). Once all the pixels have been treated, the center of each cluster was computed, giving the position of the sensors in the image (and in the image reference frame).

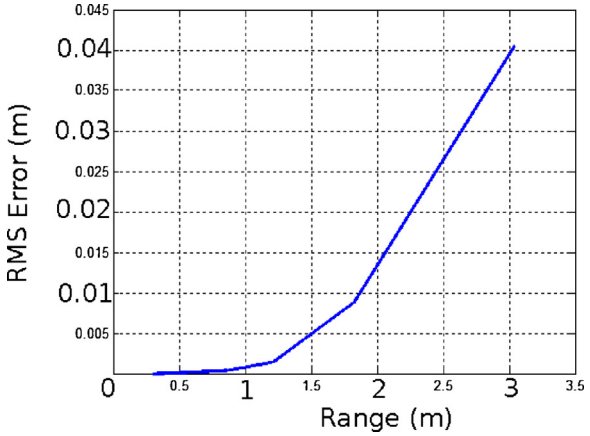


**Fig. 3.** Error of a magnetic sensor as a function of the distance to the receiver (data from Polhemus).

#### 2.6.2. Statistical analyses

The comparison between nat-PIV and ST + KLT velocity fields was processed in two steps. The first step was a consistency test: we tested for significant and systematic differences in the results given by the two methods. The second step was a direct assessment of the two methods with the results given by magnetic sensors. Each time, the velocity fields were analyzed component by component (horizontal and vertical).

Comparisons between the velocimetric methods were achieved through linear correlations and orthogonal regressions between the output of two methods $V_{ts,meth\text{-}i} = f(V_{ts,meth\text{-}j})$ (i.e. nat-PIV vs ST + KLT, and then nat-PIV vs magnetic tracking and ST + KLT vs magnetic tracking. Indeed none of the method provides negligible errors and both are considered with equal respect. Thus, there is no reason to minimize the sum of square in a preferential direction by using the usual least square regression. Regressions were thus computed by minimizing the sum of square in two directions namely by an orthogonal regression (Dagnelie, 2007).

Orthogonal regression lines (Dagnelie, 2007) were computed for each test set, as well as the correlation coefficient (noted $R_{ts}$). The slope of the line ($a_{ts}$) and the intercept ($b_{ts}$) are given by: $a_{ts} = \sigma(V_{ts,meth\text{-}i})/\sigma(V_{ts,meth\text{-}j})$ and $b_{ts} = \langle V_{ts,meth\text{-}i}\rangle - a_{ts}\ \langle V_{ts,meth\text{-}j}\rangle$ where $\sigma(V_{ts,Meth})$, $\langle V_{ts,Meth}\rangle$ are respectively the standard error and the average of the velocimetry computed by a method for a given situation. The confidence interval at 95% is noted $a_{ts,sup}$ and $a_{ts,inf}$ with $a_{ts,sup} = a_{ts}(1 + 2k_{ts} + ((1 + 2k_{ts})^2 - 1)^{1/2})^{1/2}$, $a_{ts,inf} = a_{ts}(1 + 2k_{ts} - ((1 + 2k_{ts})^2 - 1)^{1/2})^{1/2}$, $k = t^2_{1-\alpha/2}(1 - R^2_{ts})/(n - 2)$.

If the confidence interval for slopes $[a_{ts,inf}, a_{ts,sup}]$ does not include 1 then a significant bias is found between the two methods.

The slopes of the orthogonal regressions for each method and for both directions were then used as input data for the assessment of possible effects of the characteristics of the sequences (texture of the image and wind conditions) and of the processing. A preliminary one-way analysis of variance (ANOVA) was performed to test if the slope of the relation between velocimetric methods was dependent on (i) the direction of the movement (horizontal or vertical components) and (ii) the sensor number and location (for comparison with the magnetic method). Then the influence of foliage and wind conditions (see Section 2.3) were assessed through a type III two-ways ANOVA on the slopes of the regressions of each methods for both directions and sensor positions to the magnetic reference.

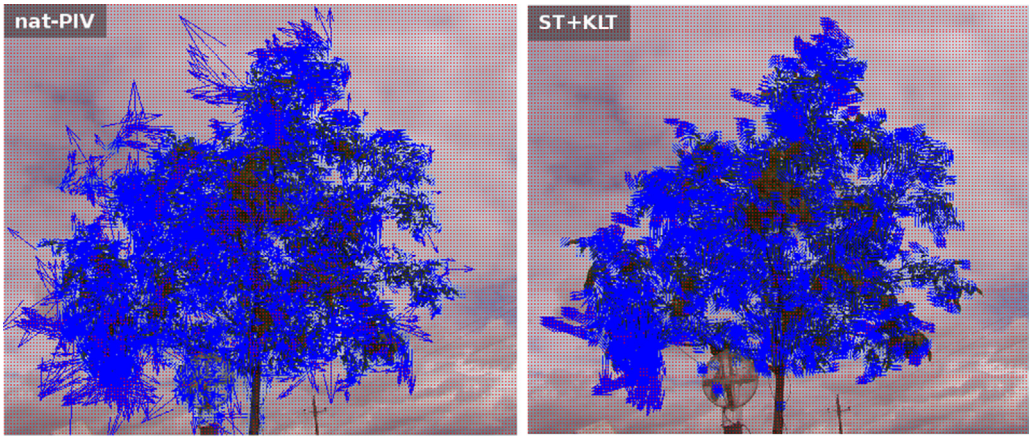


**Fig. 4.** Illustration of velocimetry fields for the situation DHighW (Dense foliage et High wind velocimetry) for nat-PIV and ST + KLT methods.

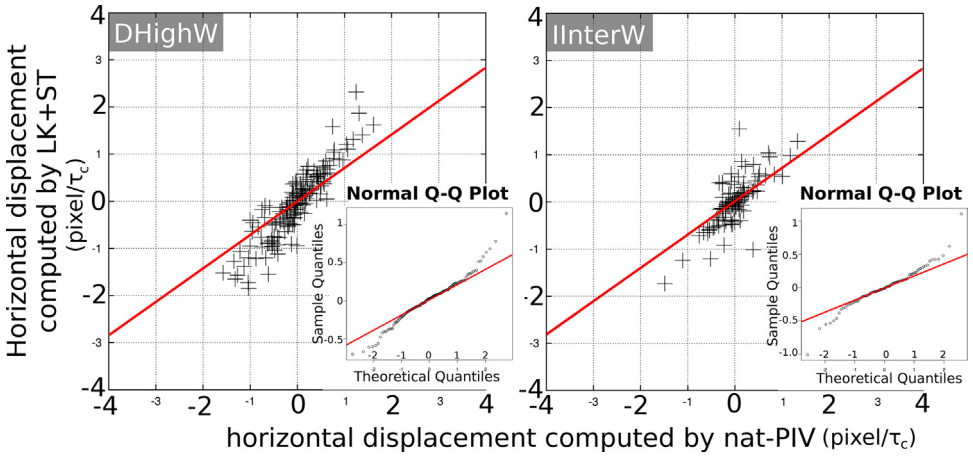


**Fig. 5.** Comparison between displacement fields computed by nat-PIV and ST + KLT for two test sets. The velocity computed by nat-PIV is superior than the one computed by ST + KLT. $\tau_c$ is the sampling time of the camera ($\tau_c = 1/25$ s).

All the statistical computations were made with MATLAB version 7.10.0 (Natick, Massachusetts: The MathWorks Inc., 2010, Statistics toolbox).

## 3. Result

### 3.1. Comparison nat-PIV/ST + KLT

Fig. 4 displays typical instantaneous velocity fields obtained for the Dense Foliage and high wind conditions, using both nat-PIV and ST + KLT (see also supplementary data).

In both cases the velocity fields described only the motion of the tree elements, and not of the background (e.g. clouds). The density of the velocity field was high, but not homogeneous, displaying some patchiness (with a slightly more pronounced patchiness for the output of ST + KLT). For both methods the central zone of the crown displayed a lower density in the velocity field. There were some "black patches" where no velocity estimates were found, but these "black patches" were of limited extent. nat-PIV tended to output some surprisingly large velocity vectors at the boundaries of the crown (outliers), whereas ST + KLT did not.

The result of the orthogonal regression of the relation $V_{ts,ST+KLT} = f(V_{ts,nat\text{-}PIV})$ were qualitatively the same for all the test sets (Fig. 5 and Table 2). There was a good linear correlation between the outputs of the two methods, with normally distributed residual errors. However this correlation and the explained variance tended to be weaker for the vertical components of the velocity vectors than for the horizontal components. Moreover, the slopes were systematically significantly inferior to 1 while the *Y*-intercept of the regression was always quite close to 0 (no systematic bias). So, the velocities computed by ST + KLT were systematically smaller than the ones computed by nat-PIV.

**Table 2**
Result of the orthogonal regressions for each velocimetry direction for the relation between nat-PIV and ST + KLT ($a_{ts}$ = slope; $a_{ts-}$ $a_{ts+}$ = limits of the confidence interval on slopes; $b_{ts}$ = *Y*-intercept and $R_{ts}$ = correlation coefficient).

| Test-set | Horizontal | | | | | Vertical | | | | |
|---|---|---|---|---|---|---|---|---|---|---|
| | $a_{ts}$ | $a_{ts-}$ | $a_{ts+}$ | $b_{ts}$ | $R^2_{ts}$ | $a_{ts}$ | $a_{ts-}$ | $a_{ts+}$ | $b_{ts}$ | $R^2_{ts}$ |
| DHighW | 0.8448 | 0.8445 | 0.8452 | 0.006 | 0.72 | 0.8216 | 0.8212 | 0.8220 | 0.008 | 0.62 |
| DMediumW | 0.8756 | 0.8752 | 0.8759 | 0.004 | 0.72 | 0.8622 | 0.8618 | 0.8626 | 0.003 | 0.59 |
| IHighW | 0.8157 | 0.8154 | 0.8160 | 0.004 | 0.69 | 0.8037 | 0.8033 | 0.8040 | 0.003 | 0.57 |
| IMediumW | 0.7124 | 0.7121 | 0.7127 | −0.004 | 0.46 | 0.7089 | 0.7085 | 0.7092 | 0.003 | 0.42 |

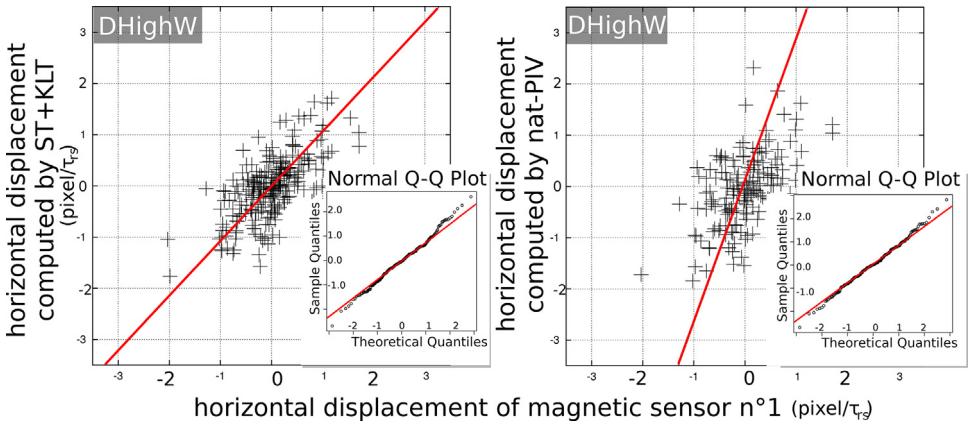


**Fig. 6.** Illustration for the situation DhighW (Dense foliage et High wind velocimetry) of the results obtained for the regressions between ST + KLT and nat-PIV vs magnetic velocimetries. The *Q*–*Q* plot (in bottom right of each graph) indicates the normality of residual. $\tau_{rs}$ is common time period shared by the magnetical and numerical measurements ($\tau_{rs}$ = 0.2 s).

The relations between nat-PIV and ST + KLT were not affected by the direction of the movement (*p*-value = 0.76). However the value of the slope was significantly influenced by the Foliage density (*p*-value < $10^{-3}$), the wind intensity (*p*-value < $5.10^{-2}$) and their interaction (*p*-value < $5 \times 10^{-2}$). A Fisher LSD post hoc test showed that when the wind intensity was high, the effect of the foliage density was lower. Consistently, the slopes obtained for the situation NullW + Inert, with no foliage and very small displacements, were the smallest ($a_{NullW+Inert}$ = 0.55).

In summary, ST + KLT velocity estimates were smaller than the ones given by nat-PIV by approx 20%. The smaller the velocity, the higher the effect of foliage density (and thus of the texture of images).

### 3.2. Comparison of optical vs magnetic velocimetric methods

When comparing the velocity field of the magnetic sensor computed using the optical velocimetric methods to the velocities computed from the magnetic tracking, highly significant linear regressions were found (Fig. 6 and Table 3). The ANOVA indicated that the slopes of ST + KLT vs Magnetic and nat-PIV vs Magnetic were statistically different (*p*-value = $2 \times 10^{-2}$).

The best fit were obtained for ST + KLT, with a mean slope of 1.09, intercepts close to 0 (mean intercept = −0.05), and correlation coefficient in the range from 0.5 to 0.9 (mean *R* = 0.75) (Table 3). However, the slope of the ST + KLT vs magnetic regression for each of the sequences analyzed was most of the time statistically different from 1 since the confidence intervals did not always contained this value (e.g. Table 3, ST + KLT sensor 1 DMediumW situation). The maximal slope was 1.336 for the IMediumW situation, and the minimum was 0.819 for the DMediumW situation. The differences to the magnetic measurement were thus up to 33% for the IMediumW situation.

The results for nat-PIV were much more biased. Indeed the slopes of the regressions of nat-PIV vs Magnetic were higher than the slopes given by ST + KLT vs Magnetic by at least 28% and further different from 1 (Table 3). High values of slope discrepancy to 1, of *Y*-intercept and poor correlation coefficients were especially observed using nat-PIV for the IHighW and IMediumW situations, due to unfiltered outliers in the velocimetry field. The differences between the nat-PIV and magnetic velocimetry were up to 700% in the IHighW modality.

In the extreme test-set NullW + Inert the slopes of the nat-PIV vs Magnetic were around 1.5 for every sensor and for every directions whereas for ST + KLT vs Magnetic the relation were closer to 1 (1.2).

For each optical method, ANOVA did not detect a relation between the slope coefficients and the sensor position (ST + KLT: *p*-value = 0.33; nat-PIV: *p*-value = 0.97), or the direction of the movement (ST + KLT: *p*-value = 0.65; nat-PIV: *p*-value = 0.96). The slope coefficient was also found to be independent of foliage density and wind intensity (for ST + KLT and nat-PIV *p*-value > 0.1) in 95% of cases.

**Table 3**
Result of the orthogonal regressions for each velocimetry direction for the relation between nat-PIV or ST + KLT and magnetic velocimetries ($a_{ts}$ = slope; $a_{ts-}$ $a_{ts+}$ = limits of the confidence interval on slopes; $b_{ts}$ = Y-intercept and $R_{ts}$ = correlation coefficient).

| Test-set | | | Wind | Hortizontal | | | | | Vertical | | | | |
|---|---|---|---|---|---|---|---|---|---|---|---|---|---|
| Method | Sensor | foliage | | $a_{ts}$ | $a_{ts-}$ | $a_{ts+}$ | $b_{ts}$ | $R^2_{ts}$ | $a_{ts}$ | $a_{ts-}$ | $a_{ts+}$ | $b_{ts}$ | $R^2_{ts}$ |
| ST + KLT | 1 | D | High | 1.068 | 0.972 | 1.175 | −0.388 | 0.43 | 1.085 | 0.984 | 1.197 | 0.251 | 0.40 |
| | 2 | D | High | 1.075 | 0.984 | 1.175 | −0.203 | 0.50 | 0.946 | 0.850 | 1.053 | 0.820 | 0.28 |
| | 1 | I | High | 0.834 | 0.781 | 0.892 | −0.389 | 0.68 | 1.108 | 1.033 | 1.188 | −0.425 | 0.66 |
| | 2 | I | High | 1.181 | 1.128 | 1.236 | 0.143 | 0.84 | 1.012 | 0.962 | 1.065 | −0.346 | 0.81 |
| | 1 | D | Medium | 1.235 | 1.129 | 1.352 | −0.350 | 0.47 | 1.164 | 1.064 | 1.272 | 0.216 | 0.49 |
| | 2 | D | Medium | 1.137 | 1.059 | 1.220 | −0.425 | 0.67 | 0.819 | 0.749 | 0.897 | −0.007 | 0.48 |
| | 1 | I | Medium | 1.192 | 1.060 | 1.339 | 0.239 | 0.34 | 1.336 | 1.209 | 1.476 | 0.292 | 0.50 |
| | 2 | I | Medium | 1.156 | 1.090 | 1.226 | −0.557 | 0.83 | 1.148 | 1.082 | 1.218 | 0.329 | 0.83 |
| nat-PIV | 1 | D | High | 2.488 | 2.197 | 2.817 | 1.604 | 0.04 | 1.346 | 1.214 | 1.492 | −1.384 | 0.34 |
| | 2 | D | High | 1.355 | 1.228 | 1.494 | 0.135 | 0.40 | 2.292 | 2.027 | 2.591 | 0.613 | 0.06 |
| | 1 | I | High | 7.494 | 6.649 | 8.446 | 7.788 | 0.01 | 1.479 | 1.347 | 1.624 | −0.571 | 0.38 |
| | 2 | I | High | 1.729 | 1.593 | 1.876 | −1.643 | 0.53 | 1.183 | 1.125 | 1.244 | −0.669 | 0.81 |
| | 1 | D | Medium | 1.917 | 1.727 | 2.127 | −0.843 | 0.30 | 1.504 | 1.356 | 1.667 | −0.363 | 0.31 |
| | 2 | D | Medium | 1.285 | 1.192 | 1.384 | −0.183 | 0.64 | 1.055 | 0.957 | 1.164 | −0.159 | 0.38 |
| | 1 | I | Medium | 2.314 | 2.017 | 2.655 | −1.342 | 0.16 | 2.377 | 2.074 | 2.724 | 0.686 | 0.18 |
| | 2 | I | Medium | 1.957 | 1.748 | 2.190 | −2.837 | 0.38 | 9.756 | 8.460 | 11.251 | 6.473 | 0.02 |

## 4. Discussion and conclusion

These experiments demonstrate that reliable and consistent estimates of dense velocity fields resulting from wind-induced motions of complex trees in natural conditions can be achieved using video recording by standard cameras, in all the situations of wind and foliage density. This was achieved in a very challenging conditions, namely a complex tree in the field, with natural lighting and changing sky background, in a sample of different weathers and seasonal foliage situations all through the year. To our knowledge this is the very first time that these methods have been systematically assessed versus a reference method for plants measurements (accuracy assessment have been performed but on simple scenes, e.g. Westerweel, 2000).

The ST + KLT method proved to always be more accurate and robust. This could not be inferred from theory. Indeed the most straightforward hypothesis was that nat-PIV would be more efficient for dense foliages, and that the ST + KLT method would only be efficient with obvious angular features such as in the leafless tree. But this is not the case. Even in conditions of dense foliage, a high density of "good features to track" were found (mostly leaf tips, bases, etc.) using ST. The ST + KLT method also proved to be quite insensitive to possible light intensity gradients set up by the heterogeneous lighting intrinsic to natural light conditions.

It may be argued that part of the behavior of the nat-PIV could be improved by using more advanced post-processing filtering than the standard one we used in this study (e.g. Vétel et al., 2011). However most of the aberrant vectors were lying at the edge of the field (i.e. edge of the crown), and this is the most difficult situation for filtering. Therefore a method that provides more consistent outputs without filtering (as does the ST + KLT) is to be preferred.

Although providing on average a non-biased estimates, ST + KLT was found to provide possible errors up to 20% along horizontal direction and up to 33% along vertical one (when compared to Magnetic tracking). The reason for this is not clear, and did not relate to any of the studied factors (wind intensity, foliage density, motion direction). However this drawback is compensated for the advantages of the ST + KLT optical velocimetric method, compared to contact methods such as magnetic tracking, inclinometer or strain gauges. Indeed none of the contact methods is able to produce such a dense field of velocity.

This study was however dedicated to the analysis of the 2D projection of the wind-induced motion of an isolated tree. Moreover, we studied cases in which the direction of the dominant wind was laying along the image, so that the drag motion should be easier to follow. Producing a 3D reconstruction of the velocity field for any wind direction is theoretically possible, but will face the usual difficulties of 3D reconstruction of trees, namely the automatic pairing of the features to track, and the problem of hidden objects. It is likely that the result will be less dense and noisier. If the wind-induced tree motions are the main target though, an alternative can be to identify vibration modes of the tree (using for example Bi Orthogonal Decomposition, e.g. Py et al., 2006) on the videos from two orthogonal cameras. Instead of matching the good feature to track one by one, the whole vibration modes in the two planes can be matched from their frequency and the global modal deformation then reconstructed. This may allow identifying branch modes, but also the modes involving the deformation of the trunk, in which all the points in the crown experience a coherent motion, to be reconstructed (see Rodriguez et al., 2008 for the description and typology of vibration modes in a walnut tree). However the direct measurement of the trunk through local measurements methods (displacement sensors, tilt meters, strain gauges, etc.) are usually easy, and will provide accurate description of the deformation of stem and main branches. So the two types of methods (optical ST + KLT velocimetry and local measurements) can easily be associated to provide an accurate and dense description of the motion and deformation of the whole tree.

A further complication may be experienced when trying to analyze plants within a dense canopy. The drawbacks here are those of any optical method (hidden parts, obstacles to step back the cameras, etc.). Optical methods may however been used to track the motion of the top of the canopy, as long as it produces a fairly flat surface (crop and grasses, young forests). Py et al. (2005, 2006) have used nat-PIV in these conditions, providing novel insights on the plant–wind interactions on top of the canopy. However their validation was crude. It is likely that they would have experienced the bias that was revealed in that study and the ST + KLT method is likely to be more reliable in these situations.

Finally, although we experienced very different cloudiness along the experiment (see Fig. 1), we cannot claimed to have investigated all the type of background. In the case of moving background (e.g. small clouds) though, the Kineplant-CRToolbox software provides tools to restrict the part of the image used to compute velocimetry fields to the vicinity of the tree. This can achieved either manually or automatically.

The ST + KLT method and the Kineplant-CRToolbox software thus provide a reliable and straightforward method for dense velocimetric measurements of wind induced movement. It is now available for use by plant biomechanics, micrometerology or mechanobiology. This should allow for developments in the experimental study of wind induced motion, and to the possibility of assessing models of plant–wind interaction. Finally the dataset produced of tree and wind velocities during this experiment is unique and may be used to assess mechanical models of wind–tree interactions with explicit architecture (e.g. Sellier et al., 2006; Rodriguez et al., 2008). Data are available on request by e-mail.

## Acknowledgments

The authors wish to thanks the anonymous reviewers for their relevant remarks and comments.

This work was supported by ANR Grant 06-BLAN-0210-02 "Chêne Roseau" involving the Ecole Polytechnique, INRIA and INRA. The authors thank S. Ploquin and P. Chaleil for technical assistance with the tree experiments.

## Appendix A. Supplementary data

Supplementary data associated with this article can be found, in the online version, at http://dx.doi.org/10.1016/j.agrformet.2013.10.003.

## References

Achim, A., Ruel, J., Gardiner, B., Laflamme, G., Meunier, S., 2005. Modelling the vulnerability of balsam fir forests to wind damage. Forest Ecol. Manage. 204, 37–52.
Baker, S., Matthews, I., 2004. Lucas-Kanade 20 years on: a unifying framework. Int. J. Comput. Vis. 56, 221–255.
Berry, P., Sterling, M., Baker, C.J., Spink, J., Sparkes, D.L., 2003. A calibrated model of wheat lodging compared with field measurements. Agric. For. Meteorol. 119, 167–180.
Bouguet, J.-Y., 2000. Pyramidal Implementation of the Lucas Kanade Feature Tracker Description of the algorithm. http://robots.stanford.edu/cs223b04/algo_tracking.pdf
Bradski, G., 2000. The OpenCV Library. Dr. Dobb's Journal of Software Tools.
Carr, Z.R., Ahmed, K.A., Forliti, D.J., 2009. Spatially correlated precision error in digital particle image velocimetry measurements of turbulent flows. Exp. Fluids 47, 95–106.
Cholemari, M.R., 2007. Modeling and correction of peak-locking in digital PIV. Exp. Fluids 42, 913–922.
Christensen, K.T., 2004. The influence of peak-locking errors on turbulence statistics computed from PIV ensembles. Exp. Fluids 36, 484–497.
Dagnelie, P., 2007. Statistique théorique et appliquée. Tome 1. Statistique descriptive et bases de l'inférence statistique. Bruxelles, De Boeck et Larcier.
de Langre, E., 2006. Frequency lock-in is caused by coupled-mode flutter. J. Fluids Struct. 22, 783–791.

de Langre, E., 2008. Effects of wind on plants. Ann. Rev. Fluid Mech. 40, 141–168.
de Langre, E., Rodriguez, M., Ploquin, S., Moulia, B., 2012. The multimodal dynamics of a walnut tree: experiments and models. J. Appl. Mech. 79 (4).
Diener, J., Reveret, L., Fiume, E., 2006. Hierarchical retargetting of 2D motion fields to the animation of 3D plant models. In: ACM SIGGRAPH/Eurographics Symposium on Computer Animation, SCA'06, September 2–4, Vienna, Austria.
Diener, J., Barbacci, A., Hemon, P., de Langre, E., Moulia, M., 2012. CR – KinePlant toolbox. In: Proceedings of the 7th International Biomechanics Conference, Clermont-Ferrand, p. 179.
Donès, N., Adam, B., 2008. PiafDigitTrack -Software to drive a Polhemus Fastrak 3 SPACE 3D digitiser and for the acquisition of plant architecture. In: UMR PIAF INRA-UBP Clermont-Ferrand.
Dupont, S., Brunet, Y., 2007. Edge flow and canopy structure: a large-eddy simulation study. Boundary Layer Meteorol. 126, 51–71.
Dupont, S., Gosselin, F., Py, C., de Langre, E., Hemon, P., Brunet, Y., 2010. Modeling waving crops using large-eddy simulation: comparison with experiments and a linear stability analysis. J. Fluid Mech. 652, 5–44.
Flesch, T.K., Grant, R.H., 1992a. Corn motion in the wind during senescence: I. Motion characteristics. Agron. J. 84, 748–751.
Flesch, T.K., Grant, R.H., 1992b. Corn motion in the wind during senescence: II. Effect of dynamic plant characteristics. Agron. J. 84, 742–747.
Gardiner, B., 2000. Comparison of two models for predicting the critical wind speeds required to damage coniferous trees. Ecol. Modell. 129, 1–23.
Gardiner, B., Byrne, K., Hale, S., Kamimura, K., Mitchell, S.J., Peltola, H., Ruel, J.C., 2008. A review of mechanistic modelling of wind damage risk to forests. Forestry 81 (3), 447–463.
Horn, B.K.P., Schunck, B.G., 1981. Determining optical flow. Artif. Intell. 17, 185–203.
Hedden, R.L., Fredericksen, T.S., Williams, S.A., 1995. Modelling the effect of crown shedding and streamlining on the survival of loblolly pine exposed to acute wind. Can. J. For. Res. 25, 704–712.
Hassinen, A., Lemettinen, M., Peltola, H., Kellomäki, S., Gardiner, B., 1998. A prism-based system for monitoring the swaying of trees under wind loading. Agric. Forest Meteorol. 90 (3), 187–194.
Lucas, B., Kanade, T., 1981. An iterative image registration technique with an application to stereo vision. In: Proceedings of the Imaging Understanding Workshop, pp. 121–130.
Lopez, D., Michelin, S., de Langre, E., 2011. Flow-induced pruning of branched systems and brittle reconfiguration. J. Theor. Biol. 284 (1), 117–124.
Moulia, B., Fournier, M., 1997. Mechanics of the maize leaf: a composite beam model of the midrib. J. Mater. Sci. 32, 2771–2780.
Moulia, B., Der Loughian, C., Bastien, R., Martin, L., Rodríguez, M., Gourcilleau, D., Barbacci, A., Badel, E., Franchel, J., Lenne, C., Roeckel-Drevet, P., Allain, J.M., Frachisse, J.M., de Langre, E., Coutand, C., Fournier-Leblanc, N., Julien, J.L., 2011. Mechanical integration of plant cells and plants. In: Wojtaszek, P. (Ed.), Mechanical Integration of Plant Cells and Plants. Springer, Berlin, Heidelberg, pp. 269–302.
Niklas, K.J., Spatz, H.-C., 2000. Wind-induced stresses in cherry trees: evidence against the hypothesis of constant stress levels. Trees Struct. Funct. 14, 230–237.
Py, C., de Langre, E., Moulia, B., Hemon, P., 2005. Measurement of wind-induced motion of crop canopies from digital video images. Agric. For. Meteorol. 130, 223–236.
Py, C., de Langre, E., Moulia, B., 2006. A frequency lock-in mechanism in the interaction between wind and crop canopies. J. Fluid Mech. 568, 425–449.
Raffel, M., Willert, C., Kompenhans, J., 2002. Particle Image Velocimetry: A Practical Guide, 1st ed. Springer, 1998, Corr. 2nd printing edition (Jun 11, 2002).
Raupach, M.R., Finnigan, J.J., Brunei, Y., 1996. Coherent eddies and turbulence in vegetation canopies: the mixing-layer analogy. Boundary Layer Meteorol. 78, 351–382.
Rudnicki, M., Silins, U., Lieffers, V.J., Josi, G., 2001. Measure of simultaneous tree sways and estimation of crown interactions among a group of trees. Trees 15, 83–90.
Rudnicki, M., Burns, D., 2006. Branch sway period of four tree species using 3d motion tracking. In: Proceedings of the 5th Plant Biomechanics Conference, pp. 25–31.
Rodriguez, M., Langre, E.D., Moulia, B., 2008. A scaling law for the effects of architecture and allometry on tree vibration modes suggests a biological tuning to modal compartmentalization. Am. J. Bot. 95, 1523–1537.
Rodriguez, M., Ploquin, S., Moulia, B., de Langre, E., 2012. The multimodal dynamics of a walnut tree: experiments and models. J. Appl. Mech. Trans. ASME 79 (4).
Sellier, D., Fourcaud, T., Lac, P., 2006. A finite element model for investigating effects of aerial architecture on tree oscillations. Tree Physiol. 26, 799–806.
Sellier, D., Fourcaud, T., 2005. A mechanical analysis of the relationship between free oscillations of Pinus pinaster Ait. saplings and their aerial architecture. Tree Physiol. 56 (416), 1563–1573.
Shi, J., Tomasi, C., 1994. Good features to track. In: Proceedings of IEEE Conference on Computer Vision and Pattern Recognition:, pp. 593–600.
Sterling, M., Baker, C.J., Berry, P.M., Wade, A., 2003. An experimental investigation of the lodging of wheat. Agric. Forest Meteorol. 119, 149–165.
Stoner, G.R., Albright, T.D., 1996. The interpretation of visual motion: evidence for surface segmentation mechanisms. Vis. Res. 36, 1291–1310.
Sveen, J.K., 2004. An introduction to MatPIV v.1.6.1. World Wide Web Internet And Web Information Systems.
Telewski, F.W., 2006. A unified hypothesis of mechanoperception in plants. Am. J. Bot. 93 (10), 1466–1476.
Vétel, J., Garon, A., Pelletier, P., 2011. Denoising methods for time-resolved PIV measurements. Exp. Fluids 51, 893–916.
Westerweel, J., 2000. Theoretical analysis of the measurement precision in particle image velocimetry. Exp. Fluids, 3–12.